Diffusion in tight confinement: A lattice-gas cellular automaton approach. I. Structural equilibrium properties

Pierfranco Demontis,[a] Federico G. Pazzona, and Giuseppe B. Suffritti
Dipartimento di Chimica, Università degli Studi di Sassari and Consorzio Interuniversitario Nazionale per la Scienza e Tecnologia dei Materiali (INSTM), Unità di Ricerca di Sassari, via Vienna, 2, I-07100 Sassari, Italy

(Received 20 September 2006; accepted 9 March 2007; published online 17 May 2007)

The thermodynamic and transport properties of diffusing species in microporous materials are strongly influenced by their interactions with the confining framework, which provide the energy landscape for the transport process. The simple topology and the cellular nature of the α cages of a ZK4 zeolite suggest that it is appropriate to apply to the study of the problem of diffusion in tight confinement a time-space discrete model such as a lattice-gas cellular automaton (LGCA). In this paper we investigate the properties of an equilibrium LGCA constituted by a constant number of noninteracting identical particles, distributed among a fixed number of identical cells arranged in a three-dimensional cubic network and performing a synchronous random walk at constant temperature. Each cell of this network is characterized by a finite number of two types of adsorption sites: the *exit sites* available to particle transfer and the *inner sites* not available to such transfers. We represent the particle-framework interactions by assuming a differentiation in binding energy of the two types of sites. This leads to a strong dependence of equilibrium and transport properties on loading and temperature. The evolution rule of our LGCA model is constituted by two operations (randomization, in which the number of particles which will be able to try a jump to neighboring cells is determined, and propagation, in which the allowed jumps are performed), each one applied synchronously to all of the cells. The authors study the equilibrium distribution of states and the adsorption isotherm of the model under various conditions of loading and temperature. In connection with the differentiation in energy between exit and inner sites, the adsorption isotherm is described by a conventional Langmuir isotherm at high temperature and by a dual-site Langmuir isotherm at low temperature, while a first order diffuse phase transition takes place at very low temperature. © *2007 American Institute of Physics*. [DOI: 10.1063/1.2721546]

I. INTRODUCTION

Microporous materials such as zeolites have found many different uses in many different areas of application ranging from catalysis to molecular sieving.[1] An important subject where researchers in this field have focused their attention is the mobility of molecules adsorbed on the inner surface of the micropore. The physics of this phenomenon is influenced by the nature of the particle-framework interactions[2] which provide the energy landscape for the transport process and therefore influences the aptitude of a particle to migrate from pore to pore. As a consequence geometric effects as pore size and pore shape along with connectivity and tortuosity should be recognized among the factors playing a major role. Despite a significant experimental and theoretical research effort, many of the diverse physical phenomena associated with diffusion in tight confinement, such as heterogeneous catalysis, biological transport, percolation, and even a dramatic change of the phase diagram,[3] are still far from being understood.[4] In essence, the diffusivity of a guest molecule will depend on the size and the shape of the channels and cages of the internal pores, related to the size and shape of the molecule itself. In addition, the number of the adsorbed molecules in each of the channels and cages will deeply modify diffusion by both chemical and steric effects. The above remarks inspire a coarse-grained description of the internal void space of a material:[5] the channels and cages connected to one another define a system of communicating cells that can contain and exchange a limited number of guest particles. Moreover, this constraint can cause a sharp separation on the time scales involved in the diffusion process: intracell motion (short times) and intercell migration (long times).[6] When the time scale of the intracell motion is negligible with respect to the time scale of the intercell migration, the physical process of diffusion can be conveniently represented as a discretized process in which at each time step particles jump from one cell into a neighboring cell. Therefore, at each time step, the only quantity to be determined is the number of particles that leave each cell and entering into the neighboring ones. This suggests that when reduced to its essential constituents the system can be represented in space as a set of structured lattice points (cells) evolving in time according to well defined rules. Following these lines we recently developed[7] a simple cellular automaton[8,9] evolving in time through a two-step rule. Focusing on a cell at a particular time step, (i) we find out how

[a]Author to whom correspondence should be addressed. Electronic mail: demontis@uniss.it

many particles will be able to try a jump into the neighboring cells, and next (ii) we perform the allowed jumps. In this way we naturally construct a chain of states corresponding to a trajectory in configuration space, where on the long run the different states emerge with the statistical weights given by the Boltzmann distribution. The ability of a particle to try a jump is conditioned by its ability to occupy an *exit site*, i.e., a site connecting the host cell to a neighboring cell. In a cell, the exit sites differ from the *inner sites* (which are not connected to neighboring cells) in binding energy. A differentiation among several types of adsorption sites, mutually differing in adsorption energy, has been shown to be a feature of most nanoporous materials,[10–13] giving rise to a strong dependence of both equilibrium and transport properties on loading and temperature.[7,14–16] For example, experimental evidences[17] have shown that in NaY zeolite benzene molecules appear to occupy two types of sites, cationic sites on the walls of the supercage and less favorable window sites in apertures between adjacent supercages, a behavior consistent with results from molecular dynamics simulations.[18]

Our model can be classified as a lattice-gas cellular automaton (LGCA) and in its first applications we are studying cases where mutual interactions between adparticles are negligible with respect to the interactions with the framework. The realistic mechanism adopted to model the elementary changes in the cage occupancy allows a dynamical interpretation of our LGCA simulation results. Our probabilistic model differs by traditional kinetic Monte-Carlo[19] (KMC) approaches in that the model is parallel, that is, all of the cells are updated simultaneously at each time step. Despite this important difference, our approach shares with the KMC method the general idea that the local properties (such as the number of molecules in each cell, diffusion barrier, and presence of other nearby molecules) determine the direction the molecule will diffuse. All of the significant physical properties are represented by a small set of parameters which rule both the tendency of molecules to migrate and the time-space correlations. The evolution algorithm is fast; therefore the model, with opportune tuning of parameters, can be used to simulate diffusion of weakly interacting particles in large microporous systems for long time scales.

In the present paper we will focus on the structural equilibrium properties of the model. In the paper that follows, denoted as Paper II, we report the dynamical properties that can be studied from the model.

II. STRUCTURE OF THE MODEL

A. The model

Our model consists of N identical, distinguishable particles diffusing in a d-dimensional hypercubic lattice $\mathcal{L}$ of $M=L^d$ cells with periodic boundary conditions. The *loading* $\langle n\rangle$ of the system is defined as the average number of particles per cell, $\langle n\rangle = N/M$.

Each cell is labeled by the coordinates of its center, $\mathbf{r}$, and can exchange particles with its $\nu=2d$ nearest-neighboring cells labeled as

$$\mathbf{r}^i = \mathbf{r} + \lambda \mathbf{e}_i, \quad i = 1, \ldots, \nu,$$

where $\mathbf{e}_1, \ldots, \mathbf{e}_{2d}$ are orthogonal unit vectors satisfying $\mathbf{e}_{i+d} = -\mathbf{e}_i$, $i=1,\ldots,d$ and λ is the fixed distance between centers of adjacent cells.

The system evolves in discrete time steps of arbitrary duration τ. Each cell, say, $\mathbf{r}$, contains $K \geqslant \nu$ distinguishable sites labeled as $(\mathbf{r},i)$, $i=1,\ldots,K$. We assume that a site can accommodate only one particle. This implies an exclusion principle so that the site $(\mathbf{r},i)$ has only two states coded by the Boolean variable $s_i(\mathbf{r},t)=1,0$ if the site is occupied or not, at time t, respectively. Therefore K is the maximum number of particles that can be contained in one cell.

We call the *configuration* of cell $\mathbf{r}$ at time t the set of instantaneous states of its sites, i.e., $\mathbf{s}(\mathbf{r},t)=\{s_i(\mathbf{r},t)\}_{i=1,\ldots,K}$. The K sites of each cell are not equivalent. We specify that in each cell $\mathbf{r}$, (a) the sites $(\mathbf{r},i)$, $i=1,\ldots,\nu$ are *exit* sites, which are available to particle transfers; (b) the sites $(\mathbf{r},i)$, $i=\nu+1,\ldots,K$ are *inner* sites, which are not available to particle transfers.

The exit sites connect the cell with its first-neighboring cells in the following way: for each $i \in [1,\nu]$, the exit site $(\mathbf{r},i)$ points toward the direction of the neighboring cell $\mathbf{r}^i$ and is connected to the site $(\mathbf{r}^i, i+d)$ (the sum $i+d$ is a sum modulo $2d$). Given the Boolean nature of the s_i's, at each time step at most one particle can migrate from one of these adjacent sites to the other one. This is equivalent to impose a *geometrical restriction* and plays the role of a constraint on the particle traffic.

We indicate as

$$n(\mathbf{r},t) = \sum_{i=1}^{K} s_i(\mathbf{r},t), \tag{1}$$

and

$$n_{\mathrm{ex}}(\mathbf{r},t) = \sum_{i=1}^{\nu} s_i(\mathbf{r},t), \tag{2}$$

respectively, the *occupancy* (local density number) and the *exit site occupancy* (number of occupied exit sites) of the cell $\mathbf{r}$ at time t. The *inner site occupancy* is obviously defined as $n_{\mathrm{in}}=n-n_{\mathrm{ex}}$.

When referring to a cell with configuration $\mathbf{s}$ instead of referring to the variables $\mathbf{r}$, t we shall use the notations $n(\mathbf{s})$ and $n_{\mathrm{ex}}(\mathbf{s})$ to denote the quantities in Eqs. (1) and (2).

We differentiate the statistical weight of the two kinds of site by assigning them a different energy (lattice gases with two nonequivalent sites were extensively studied by Chvoj *et al.*,[15] Tarasenko *et al.*,[16] and by Bhide *et al.*[20] through KMC simulations). We denote $-\varepsilon_{\mathrm{ex}}$ the energy of an exit site and $-\varepsilon_{\mathrm{in}}$ the energy of an inner site.

As a result of the choice $\varepsilon_{\mathrm{ex}} \neq \varepsilon_{\mathrm{in}}$, different configurations are differently weighted depending on the temperature T. Nontrivially loading dependent diffusion profiles will emerge as a consequence of the fact that the temperature controls the accessibility of the exit sites, therefore influencing the frequency of transfers.

Although inside of a cell all the K sites are distinguishable, in our coarse-grained approach the cell interior is not

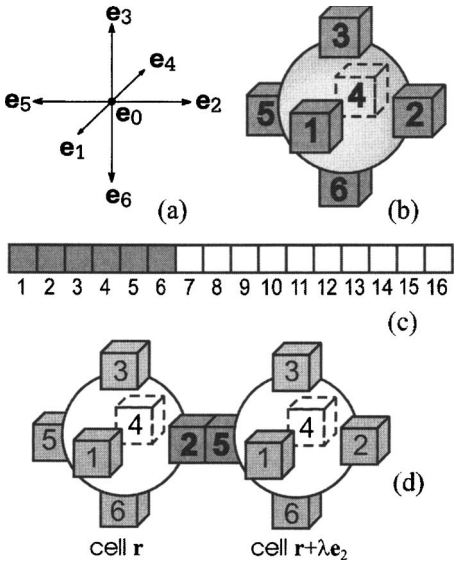

FIG. 1. (a) Sketch of the unit vectors of the lattice. In (b) and (c) two representations of a unit cell with $\nu=6$, $K=16$ are reported: (b) three-dimensional sketch and (c) string representation. In (b) gray numbered cubes represent *exit sites*, while the sphere represents the ensemble of *inner sites*. Assigned numbers establish the correspondence between exit sites in the three-dimensional (3D) sketch (gray cubes) and in the string representation (gray squares). The topology of exit sites in one cell is the same as the topology of the cells in the entire system; therefore it must be specified. The inner sites are distinguishable, but their spatial arrangement is ignored (this is why we employ a sphere for their 3D representation and white numbered squares in the string). In (d) two connected cells, named $\mathbf{r}$ and $\mathbf{r}+\lambda\mathbf{e}_2$, are represented. As can be seen, site 2 of cell $\mathbf{r}$ communicates with site 5 of cell $\mathbf{r}+\lambda\mathbf{e}_2$. The two cells can exchange particles using only these two connected sites. Since each site cannot host more than one particle, two adjacent cells can exchange at most one particle at time. This represents a *constraint* on the particle traffic.

detailed as a lattice except in the exit sites, which must have a well specified topology in order to define the connections among cells while the spatial arrangement of the inner sites is ignored (see Fig. 1). As a consequence of this assumption, the spatial position of each particle is defined as the position of its host cell in the lattice.

Moreover, we choose to *totally* neglect the time scale relative to intracell motion and to treat the particles *inside* of each cell as indistinguishable.

The physical process generated by our model is a *simultaneous* intercell random walk of all the guest particles, and the properties of this random walk are strongly influenced by the differentiation of the energies in the site, the temperature, and the loading.

B. The Hamiltonian

We suppose that the system is placed in a large heat bath at temperature T. Therefore in our model, the diffusing particles (which are equivalent and structureless, and have constant kinetic energy at constant temperature) perform a random walk in the canonical ensemble.

In a cell the occupied site i has potential energy $-\varepsilon_i=-\varepsilon_{\mathrm{ex}}$, $-\varepsilon_{\mathrm{in}}$ if it is an exit or inner site, respectively. Thus the Hamiltonian of a cell, say, $\mathbf{r}$, having the configuration $\mathbf{s}$ is defined at time t as

$$H(\mathbf{r},t)=-\varepsilon_{\mathrm{ex}}n_{\mathrm{ex}}(\mathbf{r},t)-\varepsilon_{\mathrm{in}}n_{\mathrm{in}}(\mathbf{r},t)\equiv H(n_{\mathrm{ex}},n). \tag{3}$$

As we have done for the quantities n, n_{ex}, and n_{in} in Sec. II A, when referring to a particular configuration, say, $\mathbf{s}$, we shall use the notation $H(\mathbf{s})$ to indicate the Hamiltonian of Eq. (3).

The Hamiltonian of the entire system at time t is a sum of the local Hamiltonians, $H_{\mathrm{sys}}(t)=\Sigma_{\mathbf{r}\in\mathcal{L}}H(\mathbf{r},t)$.

Given that $n_{\mathrm{in}}=n-n_{\mathrm{ex}}$, it results from Eq. (3) that the pair of observables n_{ex}, n defines a particular energy level of the cell. We indicate such a level as (n_{ex},n), and its degeneracy as $\Omega(n_{\mathrm{ex}},n)=\binom{\nu}{n_{\mathrm{ex}}}\binom{K-\nu}{n-n_{\mathrm{ex}}}$ [where we assumed that the quantity $\binom{a}{b}$ is null for $a<b$], that is the number of possible configurations having n_{ex} occupied exit sites and $n-n_{\mathrm{ex}}$ occupied inner sites. The levels satisfying $\Omega(n_{\mathrm{ex}},n)>0$ are the levels accessible to a cell with occupancy n.

III. PARTITION FUNCTIONS

The interested reader is referred to Appendixes B and C for the derivation of the formulas presented in this section.

The canonical partition function of the lattice $\mathcal{L}$ can be written as

$$Q^{\mathrm{sys}}=\sum_{\mathbf{S}}e^{-\beta H_{\mathrm{sys}}(\mathbf{S})}, \tag{4}$$

where the sum runs over all the possible configurations $\mathbf{S}$ of particles in the lattice, each with its proper energy $H_{\mathrm{sys}}(\mathbf{S})$.

In order to study the properties of the model through the computation of some probability distribution related to Q^{sys} (e.g., one can be interested in the probability distribution of finding the lattice in the energy H_{sys}), a very large number of terms have to be considered. This makes the computation an impossible task for large systems. Although Eq. (4) is a good starting point to obtain information about some thermodynamic properties (such as free energy and chemical potential), partition functions restricted to a single cell are to be preferred to define the statistical distributions the model obeys. If the correlations among different cells are negligible (and this is the case for the model considered here), and if the lattice contains a large number of cells, then such partition functions will provide information about the equilibrium properties of the entire system.

The conditional probability distribution $P^{\mathrm{eq}}(n_{\mathrm{ex}}|n)$ of finding a cell with n_{ex} occupied exit sites given that its occupancy is n reads

$$P^{\mathrm{eq}}(n_{\mathrm{ex}}|n)=\frac{\Omega(n_{\mathrm{ex}},n)e^{-\beta H(n_{\mathrm{ex}},n)}}{Q^{\mathrm{cell}}(n)}, \tag{5}$$

where $Q^{\mathrm{cell}}(n)=\Sigma_{n_{\mathrm{ex}}=0}^{\nu}\Omega(n_{\mathrm{ex}},n)e^{-\beta H(n_{\mathrm{ex}},n)}$ is the partition function of a closed cell. The probability $P^{\mathrm{eq}}(n_{\mathrm{ex}}|n)$ is independent of the loading $\langle n\rangle$.

The probability of a cell to have occupancy n, denoted $f^{\mathrm{eq}}(n)$, is given by

$$f^{\mathrm{eq}}(n)=\frac{Q^{\mathrm{cell}}(n)e^{\beta\mu n}}{Z}, \tag{6}$$

where $Z=\Sigma_{n=0}^{K}Q^{\mathrm{cell}}(n)e^{\beta\mu n}$ is the cellular (grand-canonical) partition function of the single cell, with μ as the chemical

potential. In Appendix B we show that for the model system Z reads

$$Z=(1+e^{\beta(\mu+\varepsilon_{ex})})^{\nu}(1+e^{\beta(\mu+\varepsilon_{in})})^{K-\nu}, \tag{7}$$

and that the thermodynamic equilibrium of our model is represented by a dual-site Langmuir isotherm:[11]

$$\langle n\rangle=\nu\frac{e^{\beta\varepsilon_{ex}}\lambda_a}{1+e^{\beta\varepsilon_{ex}}\lambda_a}+(K-\nu)\frac{e^{\beta\varepsilon_{in}}\lambda_a}{1+e^{\beta\varepsilon_{in}}\lambda_a}, \tag{8}$$

where ν is the capacity for adsorption in the exit sites, $K-\nu$ is the capacity for adsorption in the inner sites, $\lambda_a=e^{\beta\mu}$ is an absolute activity, and $e^{\beta\varepsilon_{ex}}$, $e^{\beta\varepsilon_{in}}$ play the role of the equilibrium constants for adsorption in the exit sites and in the inner sites, respectively. In Eq. (8) we recognize the probability of an exit site to be occupied, ρ_{ex}, and the probability of an inner site to be occupied, ρ_{in}, defined as

$$\rho_{ex}=\frac{e^{\beta\varepsilon_{ex}}\lambda_a}{1+e^{\beta\varepsilon_{ex}}\lambda_a},\quad \rho_{in}=\frac{e^{\beta\varepsilon_{in}}\lambda_a}{1+e^{\beta\varepsilon_{in}}\lambda_a}. \tag{9}$$

Inserting Eq. (7) in Eq. (6) and using the relations in Eq. (9) one obtains the following probability distribution of occupancies:

$$f^{eq}(n)=\sum_{n_{ex}=0}^{\nu}\binom{\nu}{n_{ex}}(\rho_{ex})^{n_{ex}}(1-\rho_{ex})^{\nu-n_{ex}} \times\binom{K-\nu}{n-n_{ex}}(\rho_{in})^{n-n_{ex}}(1-\rho_{in})^{K-\nu-n+n_{ex}}, \tag{10}$$

which arises from the composition of the probability distributions in two subsystems (of exit and inner sites, respectively) exchanging particles.

When the temperature is infinite, then $Z=(1+\lambda_a)^K$ and Eq. (8) reduces to the single-site Langmuir isotherm $\langle n\rangle=K\lambda_a/(1+\lambda_a)$. For the equilibrium distribution f^{eq}, this is the same as to consider $\varepsilon_{in}=\varepsilon_{ex}$, so that the system is trivially microcanonical and the mutual exclusion is the only restraint to the particle distribution in the lattice. Therefore the distribution f^{eq} converges to a hypergeometric distribution,[6] denoted f^{hyp} (see Appendix C for details).

On the other hand, the entire system is canonical when $\varepsilon_{in}\neq\varepsilon_{ex}$. In this case energy effects add to the mutual exclusion; therefore in general $f^{eq}\neq f^{hyp}$ for $T<\infty$.

The *reduced variance*, $\sigma^2/\langle n\rangle$ (where σ^2 is the variance of the occupancy distribution f^{eq} calculated at the loading $\langle n\rangle$), can be interpreted as an indicator of the thermodynamic tendency of a cell to accept a new particle. For large systems, we have that

$$\lim_{\langle n\rangle\to 0}\sigma^2/\langle n\rangle=1, \tag{11}$$

which means that in the limit of zero loading all cells are available to accept a new particle, while

$$\sigma^2/\langle n\rangle|_{\langle n\rangle=K}=0, \tag{12}$$

indicating that at the maximum loading all cells are saturated and as a consequence no cell can host a new particle.

When $\varepsilon_{in}=\varepsilon_{ex}$ (or, equivalently, the temperature is infinite), we obtain $1-\langle n\rangle/K$ for the reduced variance of a large system. Therefore, because all sites are equivalent, when the system saturates the thermodynamic tendency of a cell to accept a new particle linearly decreases with the loading $\langle n\rangle$.

IV. TIME EVOLUTION

The evolution rule follows the scheme of the randomization-propagation dynamics typical of LGCA models,[9] i.e., at each time step.

- A randomization changes the internal configuration of each cell (treated as a closed system) according to its present state only and acting simultaneously and independently on each cell.
- A propagation opens simultaneously all of the cells of the lattice to their respective neighborhoods allowing simultaneous particle transfers between adjacent cells.

Inside of each cell, the randomization determines how many particles will access the exit sites by mapping the input configuration $\mathbf{s}$ of the cell onto the output configuration $\mathbf{s}^R$ with probability $R(\mathbf{s}\to\mathbf{s}^R)$. This operation preserves the occupancy of the cell while its energy could be modified. At each time step all the cells perform the randomization simultaneously and independently from each other; therefore the randomization will cause in general a change in the energy of the entire system.

In order to ensure that the system reaches the equilibrium distribution in the long-time limit, this operation must satisfy the microscopic reversibility. In Appendix A we report in detail how this requirement is satisfied in our model.

In our previous work[7] we adopted a randomization rule consisting on a sequence of microscopically reversible Arrhenius-activated jumps of the guest particles from site to site inside of each cell. Even if this procedure ensures equilibrium in the long-time limit, it introduces time correlations in the particle random walk due to its sequential nature.

In order to generate an uncorrelated random walk, in this paper we focus on a randomizator which maps an input configuration $\mathbf{s}$ into an output one $\mathbf{s}^R$ with probability equals to the equilibrium conditional probability of a cell to be in a particular configuration $\mathbf{s}^R$ given that its occupancy is $n(\mathbf{s})$:

$$R(\mathbf{s}\to\mathbf{s}^R)=P^{eq}(\mathbf{s}^R|n(\mathbf{s}))=\frac{e^{-\beta H(\mathbf{s}^R)}}{Q^{cell}(n(\mathbf{s}))}, \tag{13}$$

which satisfies $n(\mathbf{s})=n(\mathbf{s}^R)$. Of course, the randomization trivially satisfies the detailed balance $P^{eq}(\mathbf{s}|n)R(\mathbf{s}\to\mathbf{s}^R)=P^{eq}(\mathbf{s}^R|n)R(\mathbf{s}^R\to\mathbf{s})$.

Each cell is simultaneously and *independently* randomized at each time step. The randomization selects the output configuration regardless of the input one, provided that the operation preserves the cell occupancy. Therefore, once $\mathbf{s}^R$ has been defined, inside of each cell we must redistribute randomly the particle identities into the occupied sites. This is consistent with the choice of totally neglecting the intracell motion time scale. The randomization operation is summarized in Fig. 2.

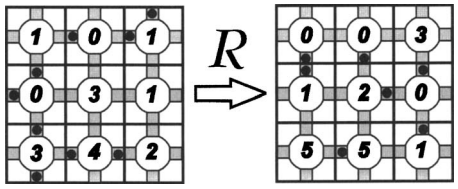

FIG. 2. The randomization (two-dimensional representation). During this operation, each cell is treated as a closed, independent canonical system. The input configuration (left) is mapped onto an output one (right) following an equilibrium criterion (see text for details). The dots represent particles in the exit sites, and the numbers represent particles in the inner sites. The total number of particles in each cell is given by the sum of the particles in the exit and inner sites. From the figure it is easy to verify that during randomization the number of particles in each cell is invariant.

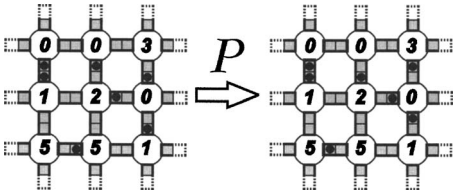

FIG. 3. The propagation (two-dimensional representation). During this operation, each pair of adjacent exit sites is treated as a closed, independent canonical system. In it, if only one exit site is occupied, then the occupying particle will jump into the other exit site with probability κ, here assumed as 1. If both exit sites are empty or occupied, then nothing occurs.

The propagation allows the intercell transfers. Let us consider two adjacent cells, say, $\mathbf{r}$ and $\mathbf{r}^i$. During propagation, they exchange a particle with probability

$$p^P(s_i(\mathbf{r}) \leftrightarrow s_{i+d}(\mathbf{r}^i)) = [s_i(\mathbf{r}) + s_{i+d}(\mathbf{r}^i) - 2s_i(\mathbf{r})s_{i+d}(\mathbf{r}^i)]\kappa_0 A e^{-\beta\varepsilon_{\mathrm{ex}}}. \quad (14)$$

This is the probability of the states $s_i(\mathbf{r})$ and $s_{i+d}(\mathbf{r}^i)$ to be swapped, as indicated by the symbol $\leftrightarrow$. As can be seen, the propagation involves uniquely independent pairs of adjacent exit sites. Since there is no interaction between exit and inner sites, this operation preserves the energy both locally and globally. Moreover, since the propagation probability p^P is symmetric, i.e.,

$$p^P(s_i(\mathbf{r}) \leftrightarrow s_{i+d}(\mathbf{r}^i)) = p^P(s_{i+d}(\mathbf{r}^i) \leftrightarrow s_i(\mathbf{r})), \quad (15)$$

there is no net drift in the particle motion, and the probability of a jump equals the probability of the reverse jump. In Eq. (14) $A=\exp(\beta \min(\varepsilon_{\mathrm{ex}}, \varepsilon_{\mathrm{in}}))$ while κ_0 is a real number in the interval (0, 1] acting as an additional barrier on intercell migration. Further details about these kinetic parameters can be found in our previous work about this model.[7] The propagation operation is summarized in Fig. 3.

V. RESULTS OF THE SIMULATIONS

We mapped our LGCA on an Linde Type A (LTA) zeolite, the ZK4, whose framework satisfies the topology requirements of the model illustrated here.[21] This system consists in a simple cubic array of nearly spherical cavities with an internal radius of ~5.7 Å connected to six neighboring cavities (therefore $\nu=6$) by nearly circular windows of ~4.2 Å in diameter. We assume that each cavity can host a maximum of 16 particles (therefore $K=16$). Where not explicitly indicated, in this work all the simulations were performed on a cubic grid of 16^3 cells. To speed up the simulations the factor κ_0 in the propagation probability [see Eq. (14)] has been set as $\kappa_0=1$. In this paper we explore how our LGCA describes equilibrium properties in restricted geometries with energetically inhomogeneous binding sites for adsorbed molecules. We use our LGCA to examine the influence of site energy heterogeneity by investigating competitive adsorption of guest molecules at different sites. Following the lines of Bhide *et al.*[20] we choose the energy parameters as $\varepsilon_{\mathrm{ex}}=10$ kJ/mol and $\varepsilon_{\mathrm{in}}=20$ kJ/mol. The choice to differentiate two types of site into each cell arises from the experimental evidence of two different types of adsorption locations in various zeolites,[11] or more generally, of n types of sites differing in their ability to bind a guest species.[10] The Langmuir model[22] is often used to describe equilibrium adsorption in zeolites. The particles do not interact except by excluding each other from the adsorption sites and one assumes that all sites are capable of holding at most one molecule each. Moreover, while in the simple Langmuir model all sites are equal, the introduction of different types of sites leads to different equilibria, corresponding to adsorption processes in pores of different binding energies. Since each equilibrium can be represented by a single Langmuir isotherm, the adsorption isotherm for n simultaneous equilibria is well reproduced by an n-site Langmuir isotherm.[10] This result has been confirmed by molecular dynamics and grand-canonical Monte Carlo simulations,[12] and has also been used in KMC models[13] to take into account the loading dependence of the self-diffusion coefficient in the study of diffusion in zeolites. In our model we differentiate the adsorption energies of the sites in order to mimic the real situation in which different adsorption locations in the cavity influence the ways a particle have access to a window (to reach an exit site, in our model) and then migrate into the adjacent cavity.

In comparison with previous lattice models of adsorption in zeolites,[20] we stress that in our simulations we replaced the crystal lattice with a three-dimensional network of cells, and that in each cell the energies of the adsorption sites and the maximum occupation number are closer to the values experimentally observed in real systems.[23,24] Moreover it is important to remark that our methodological approach is different from the strategy adopted by previous KMC simulations.[25] In our LGCA the temporal evolution of the system occurs synchronously that means a synchronous update of the occupation numbers of all cells.

Each simulation started from a random distribution of particles. After 20 000 time steps of equilibration, we observed the evolution of the system during a time interval ranging from 10^5 to 10^8 time steps, depending on the statistical accuracy required to compute the averages of interest. We performed simulations at various temperatures. The data for the case of $T \to \infty$ are obtained from simulations with $\varepsilon_{\mathrm{ex}}=\varepsilon_{\mathrm{in}}$.

A. Equilibrium distributions

A fluid adsorbed in a zeolite shows a spatially varying density. This is the key to characterize intracrystalline mass

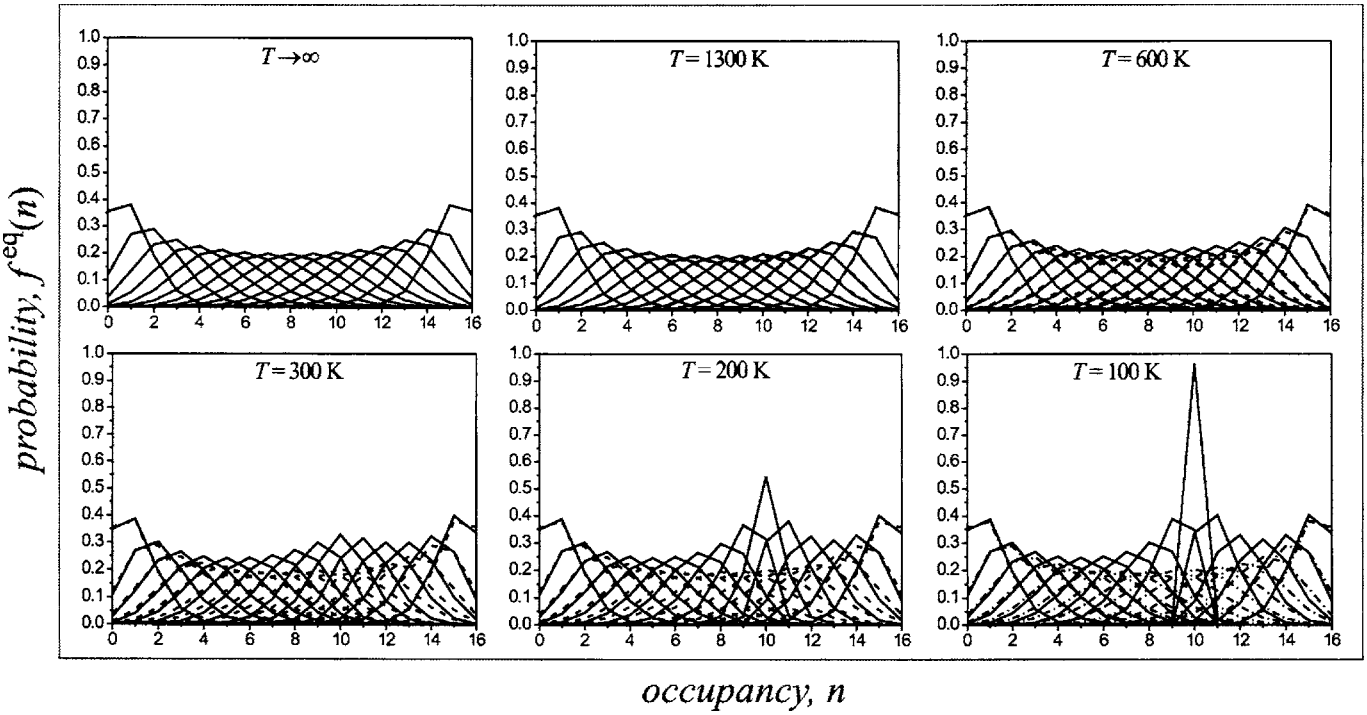

FIG. 4. The occupancy distributions f^{eq} (straight lines) computed from Eq. (10) for loadings $\langle n\rangle = 1, \ldots, 15$ at various temperatures are shown in comparison with the hypergeometric distributions f^{hyp} (dashed lines).

transport and adsorption. If we wish to develop the thermodynamics of this strongly inhomogeneous fluid we need a theory to predict how the sorbed particles distribute themselves into the inner void space that make up the zeolitic host. This probability distribution of particles over independent subvolumes[26] is a quantity that can be related to different interesting information about the system.[27] In a comprehensive theory, factors such as the finite size of the particles (which gives rise to the excluded volume effects) and the interaction forces between the fluid particles and the zeolitic host must be taken into account. Furthermore, at this molecular level of resolution, averaged properties and fluctuations turn out to be intimately related and equally important. In this field Xenon-129 NMR spectroscopy has been used under a variety of experimental conditions as a versatile tool to directly measure the fluctuations and the spatial correlations typical of guest particles in confined systems.[28] It has been possible to determine many different features of molecular dispersion within zeolite cavities and it has been noted that care must be taken in assuming a specific type of distribution.

In this paper we studied the distribution of the adsorbate in the lattice in terms of the probability $f^{eq}(n)$ of finding exactly n particles within a cell. The equilibrium distributions P^{eq} and f^{eq} computed from simulations are in perfect agreement with Eqs. (5) and (10). We plotted in Fig. 4 the f^{eq} for various temperatures and integer loadings along with a strictly statistical distribution (hypergeometric distribution, f^{hyp}) derived by Guemez and Velasco,[29] which assumes that the sorbed particles occupy mutually exclusive lattice sites in the cells. As can be seen the computed distributions differ from the hypergeometric distribution. The deviations from this statistical model can be explained by the presence of two energetically different sorption sites. Because the energy parameters ε_{in}, ε_{ex} are *constant* in space and time, the maximum value of f^{eq} always corresponds to the loading $\langle n\rangle$ but the fluctuations of the occupancy n of each cell around this value depend on the temperature. By increasing the temperature the distinction between the hypergeometric distributions and the calculated ones becomes less evident, because the energy difference between inner and exit sites becomes less important and the excluded volume effect tends to prevail (details about the convergence of the occupancy distribution f^{eq} to the hypergeometric f^{hyp} at high temperature can be found in Appendix C). The same energy difference is responsible of the behavior of the system at very low temperature.

It is interesting to observe on what grounds our measured distributions cannot be reproduced by the hypergeometric ones. We shall refer to our case study reported in Fig. 4, with $K=16$ and $\nu=6$. A symmetry relation between the hypergeometric curves exists. This means in our case that the distributions f^{hyp} calculated at the loadings $\langle n\rangle$ and $16-\langle n\rangle$ are mirror images. The calculated distribution deviates from the hypergeometric in the following ways: decreasing the temperature causes the curves no longer to be related by symmetry, and an increasing peak for $\langle n\rangle = 10$ appears. In the limit of 0 K two well defined regions emerge. The first one is a set of hypergeometric distributions going from loading 0 up to 10, while the second is again a set of hypergeometric distributions going from loading 10 up to 16 (details about the convergence of the occupancy distribution f^{eq} to two hypergeometrics f_{in}^{hyp} and f_{ex}^{hyp} in the limit of 0 K can be found in Appendix C). This seemingly contradictory result is again a sign of the presence of two energetically different sorption

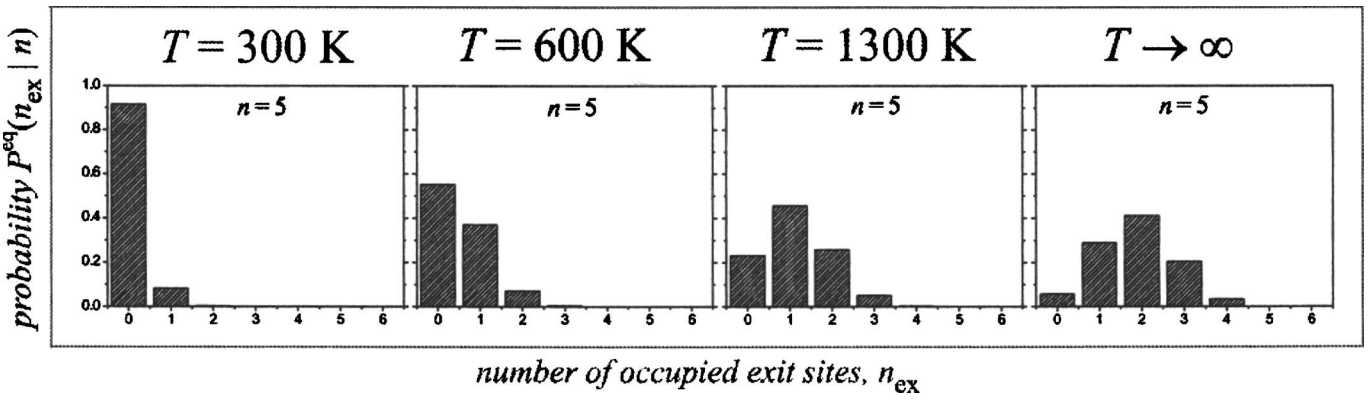

FIG. 5. Conditional probability $P^{eq}(n_{ex}|n)$ for $n=5$ at various temperatures. For low temperatures the particles tend to occupy preferably the inner sites, so $P^{eq}(n_{ex}|n)$ is significant only for the lowest possible values of n_{ex}. Therefore the accessibility of the exit sites is low. As T increases, accessibility of exit sites also increases and higher values of n_{ex} become possible.

sites where $\varepsilon_{ex}<\varepsilon_{in}$. In the limit of 0 K the first region includes the set of the equilibrium distributions on the ten equivalent inner sites while the second includes the distributions on the six energetically higher exit sites. Though in this study the interaction forces between the sorbed particles have been completely neglected, we have proven how an asymmetry in the energy of the sorption sites is enough to deeply modify the molecular distribution over the zeolitic cavities markedly expanding the temperature effects.

The temperature sensitiveness of the single cell is well represented by the behavior of the conditional probability $P^{eq}(n_{ex}|n)$ with respect to temperature. In Fig. 5 the conditional probability distribution $P^{eq}(n_{ex}|n)$, $n_{ex}=0,\ldots,\nu$ defined in Eq. (5) is plotted at various temperatures for $n=5$. At $T=300$ K, $P^{eq}(n_{ex}|n)$ is significant only for the lowest possible values of n_{ex} because the particles tend to occupy preferably the inner sites so that the states with high values of n_{ex} are rarely populated. Under such conditions the accessibility of the exit sites is low. They will become more accessible by increasing the temperature until $T\to\infty$ where the distribution $P^{eq}(n_{ex}|n)$ reaches the hypergeometric form $\binom{\nu}{n_{ex}}\binom{K-\nu}{n-n_{ex}}/\binom{K}{n}$.

As can be seen from Fig. 6, by lowering the temperature one reduces the thermodynamical tendency of a cell to accept a new particle. The nonlinear trend of the reduced variance for $T<\infty$ reflects the difference in thermodynamic properties between the two types of site in the system.

An important property of the model is that, on sufficiently large grids and far from critical conditions, the spatial correlations are negligible. To evaluate the degree of correlations among neighboring cells, away from the phase transition (see next section) we computed from simulations the static structure factor S defined as[30] $S(\mathbf{r},\mathbf{r}')=\langle\delta n(\mathbf{r})\delta n(\mathbf{r}')\rangle$, where the occupancies $n(\mathbf{r})$ and $n(\mathbf{r}')$ are evaluated at the same time step. Following Jameson[31] another simple way to keep track of spatial correlations is to compute the probability $g(m,n)$ of finding a cell of occupancy n in the neighborhood of a cell of occupancy m. Evaluating S and the distribution g for a large number of configurations near equilibrium, we find $S(\mathbf{r},\mathbf{r}')\approx 0$ for $\mathbf{r}\neq\mathbf{r}'$, and $g(m,n)\approx f^{eq}(n)$ for all values of m,n. Therefore, in this first formulation of our LGCA, spatial correlations are negligible and the occupancies are distributed in the same way both locally and globally.

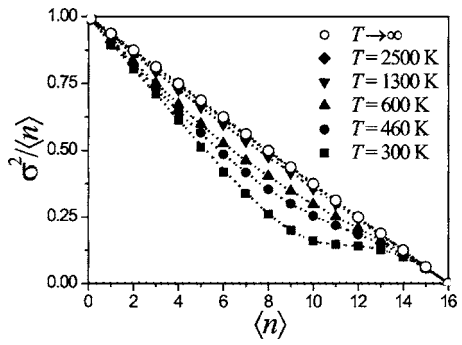

FIG. 6. Reduced variance as a function of loading at various temperatures.

B. Diffuse phase transition

When $\varepsilon_{in}\neq\varepsilon_{ex}$ the system can be divided in two subsystems.[15] The first one is the subsystem of exit sites, characterized by the energy $-\varepsilon_{ex}$. The second one is the subsystem of inner sites, characterized by the energy $-\varepsilon_{in}$. When the term $|\varepsilon_{in}-\varepsilon_{ex}|/k_BT$ increases, then the exchanges between the two subsystems become increasingly difficult. In this work we explored the case of $\varepsilon_{ex}<\varepsilon_{in}$: that is, the inner sites are the most binding. Therefore, when $T<\infty$ the particles will prefer to occupy the inner sites. At sufficiently low temperature and below some particular loading $\bar{n}_0$, the particles will mostly occupy the inner sites. The system will behave predominantly as an isolated subsystem of inner sites. The loading $\bar{n}_0$ is a loading around which the inner sites are almost all occupied. Above $\bar{n}_0$ the particles begin to fill the exit sites and, because the subsystem of inner sites is almost saturated, the transition between the two phases occurs so that the system starts to behave predominantly as the isolated subsystem of exit sites. Therefore the phase transition causes a change in the properties of the system. At *very* low temperature ($T\to 0$) the phase transition occurs precisely at the loading $\bar{n}_0=K-\nu$, where the thermodynamic properties of the system undergo a net change. Therefore in such a case we can define the transition as a *point transition*.[15]

If the temperature is *not* very low the change in properties caused by the phase transition is smooth and we cannot

locate precisely the value of $\bar{n}_0$. Instead, we can localize it in a loading interval around $\langle n\rangle = K-\nu$, that is,

$$K-\nu-\delta<\bar{n}_0<K-\nu+\delta,$$

with $\delta>0$. Therefore one can say that the system undergoes a *diffuse phase transition*.[15] Decreasing the temperature, δ diminishes and the transition becomes more definite. We observed how the phase transition takes place first calculating the chemical potential at two temperatures $T=300$ K and $T=100$ K. Each subsystem has its own partition function

$$Q_\alpha(N_\alpha)=\binom{M_\alpha}{N_\alpha}\exp\left(\frac{N_\alpha\varepsilon_\alpha}{k_BT}\right), \tag{16}$$

where $\alpha=$ex for the subsystem of the exit sites and $\alpha=$in for the subsystem of the inner sites. Therefore $M_{ex}=M\nu$ is the total number of exit sites, and $M_{in}=M(K-\nu)$ is the total number of inner sites in the lattice. N_α indicates the number of occupied sites of the α subsystem when the entire system is *at equilibrium*. We can compute the free energy of the α subsystem through

$$F_\alpha(N_\alpha)=-k_BT\ln Q_\alpha(N_\alpha), \tag{17}$$

and the chemical potential through

$$\mu_\alpha(N_\alpha)=\frac{\partial F_\alpha(N_\alpha)}{\partial N_\alpha}. \tag{18}$$

Using Stirling's approximation for large systems and noting that $\rho_{ex}=N_{ex}/M_{ex}$ and $\rho_{in}=N_{in}/M_{in}$ are the fractions of occupied sites in the exit and inner subsystems, respectively, we find

$$F_\alpha(N_\alpha)=-k_BTM_\alpha\left[\frac{\rho_\alpha\varepsilon_\alpha}{k_BT}-\rho_\alpha\ln\rho_\alpha-(1-\rho_\alpha)\ln(1-\rho_\alpha)\right], \tag{19}$$

for the free energy and

$$\mu_\alpha(N_\alpha)=-\varepsilon_\alpha+k_BT\ln\left(\frac{\rho_\alpha}{1-\rho_\alpha}\right), \tag{20}$$

for the chemical potential. Because N_{ex}, N_{in} are equilibrium values, the relation

$$\mu_{ex}(N_{ex})=\mu_{in}(N_{in}) \tag{21}$$

is satisfied. From Eq. (20) the equilibrium condition (21) implies

$$\frac{\rho_{ex}(1-\rho_{in})}{\rho_{in}(1-\rho_{ex})}=\exp\left(-\frac{\Delta\varepsilon}{k_BT}\right), \tag{22}$$

where $\Delta\varepsilon=\varepsilon_{in}-\varepsilon_{ex}$. Therefore, we can evaluate the chemical potential through the observables ρ_{ex} and ρ_{in} and using Eq. (20). Such observables are reported in Fig. 7 as functions of the loading at various temperatures, in order to visualize how the system splits in two subsystems: (i) for $T\to\infty$ the fractions ρ_{ex} and ρ_{in} increase in the same way (i.e., as $\rho=\langle n\rangle/K$); (ii) for $T<\infty$, the two fractions are equal only at $\langle n\rangle=0$ and K, while for all the other loadings $\rho_{ex}<\rho_{in}$ since the particles occupy preferably inner sites; (iii) for $T\to0$, we have $\rho_{ex}=0$ until ρ_{in} reaches the value of 1 at loading $K-\nu$, then ρ_{in} stops varying and ρ_{ex} increases from 0 to 1.

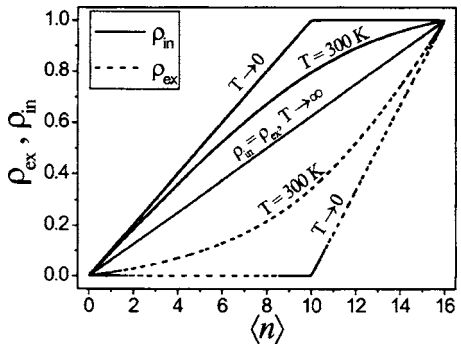

FIG. 7. Partial loading ρ_{ex} of the subsystem of exit sites (solid line) and partial loading ρ_{in} (dashed line) of the subsystem of inner sites plotted together with respect to the total loading $\langle n\rangle$ at various temperatures. For very high temperatures ($T\to\infty$) they increase in the same way because the two subsystems are equivalent. For low temperatures the two subsystems become very different; therefore the partial loadings increase with $\langle n\rangle$ in different ways.

As can be seen in Fig. 8, the phase transition at low temperature produces a singularity in the plot of μ vs $\langle n\rangle$ (i.e., the inverse plot of the adsorption isotherm). Since the variance and the chemical potential are connected by Eq. (B9) (see Appendix B), in the same conditions the reduced variance of f^{eq} exhibits a cusp.

This behavior is a feature of all systems having two (or more) distinct adsorption locations. Of course, the inverse plot of Fig. 8 is the dual-site Langmuir isotherm[32] of Eq. (8). In general, a system having n different adsorption sites will separate, at low temperatures, into n subsystems, and increasing the loading from zero to the saturation limit it will undergo $n-1$ diffuse phase transitions.

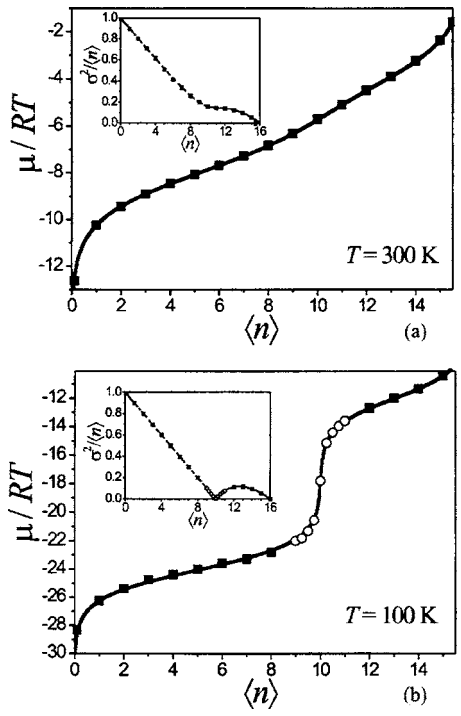

FIG. 8. The chemical potential and (in the insets) the reduced variance for $T=300$ K (top) and $T=100$ K (bottom). The simulations were performed on a grid of 32^3 cells for running times of 10^5 time steps (black squares) and of 10^8 time steps (white circles). Solid lines are fits through Eq. (8). μ is in units of kJ/mol.

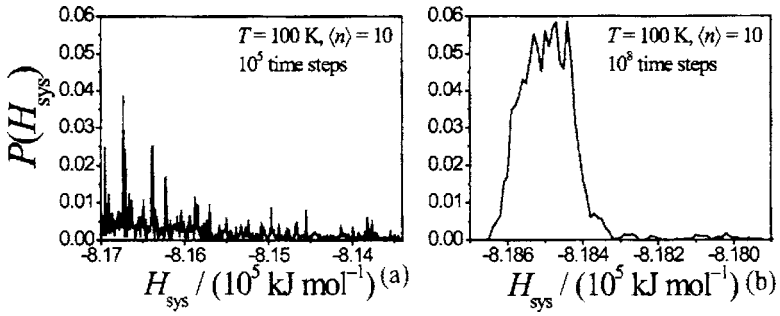

FIG. 9. The energy distributions around the phase transition ($T=100$ K, $\langle n \rangle = 10$) for a system with $M=16^3$ cells. The distribution was computed averaging over 10^5 time steps in (a) and over 10^8 time steps in (b) (see text for further details).

In Fig. 9 the energy distribution $P(H_{sys})$ (that is, the probability of finding the entire system in the energy H_{sys}) is reported for differently long simulations at low temperature. As can be seen, in the proximity of a phase transition our LGCA manifests its inherently noisy nature, and averaging over this statistical noise requires massive calculations.[33]

Since the global system is canonical, we can obtain the molar specific heat per cell at constant volume, $C_{V,m}$, from the energy distribution $P(H_{sys})$. Indicating the variance of $P(H_{sys})$ per cell as

$$\sigma_H^2 = \frac{1}{M} \sum_{H_{sys}} (H_{sys} - \langle H_{sys} \rangle)^2 P(H_{sys}), \tag{23}$$

if H_{sys} is in units of J mol^{-1} we obtain $C_{V,m} = \sigma_H^2 / RT^2$, where R is the constant of gas in units of J mol^{-1} K^{-1}. The shape of the specific heat as a function of loading is shown in Fig. 10. At $T=100$ K we observe a maximum of $C_{V,m}$ at $\langle n \rangle = K - \nu$, whose sharpness increases with $T \to 0$. This behavior of the specific heat confirms the existence of a first order diffuse phase transition in our system.

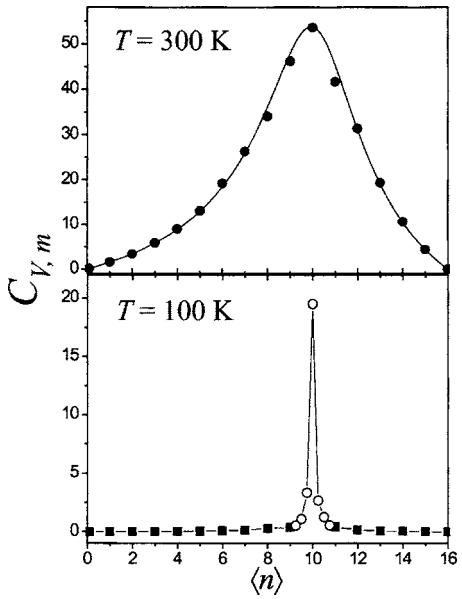

FIG. 10. The molar specific heat per cell for $T=300$ K (top) and $T=100$ K (bottom). Black squares and white circles indicate simulations 10^5 and 10^8 time steps long, respectively.

VI. CONCLUSIONS

This paper aims to contribute in addressing the problem of bridging large time and length scale gaps in simulating properties of particles adsorbed in microporous materials. For this purpose we introduced a new simulation approach based on a discrete description of the α cages of a ZK4 zeolite represented as structured lattice points (cells). The unit length scale coincides with the α-cage diameter and the interaction between particles and framework is defined using a coarse-grained description of the inner-surface forces. Basically, we replace the zeolite framework with a cubic lattice of communicating cells. Since it has been shown that the adsorption locations of several zeolites may differ in their ability to bind the adparticles and to permit intercell transfer, we differentiate the adsorption sites in each cell by giving them not only a different adsorption energy but also a different ability to transfer adparticles to neighboring cells. While retaining the essential physics of atomistic simulation our approach boosts the computational speed in predicting the equilibrium properties of a microporous material on very large scale and observation time. In our LGCA, the entire network of cells constitutes a time-space discrete canonical ensemble, while the single cell obeys to the statistics of a grand-canonical ensemble. The model evolves in time by combining two Monte Carlo operations *locally* applied to all cells simultaneously and satisfies detailed balance by providing a reversible (in probabilistic sense) path for the energy of the system between two consecutive time steps. In this approach the evolution of the system is parallel. Moreover, this framework allows to gain in computational speed by updating each cell through a dynamics of states rather than a dynamics of particle jumps. The equilibrium distributions of states and thermodynamic properties are temperature sensitive and ruled by the difference in energy between the exit sites (allowing particle transfers) and the inner sites (not allowing particle transfers). Lowering the temperature enhances the difference in statistical weights of the two kinds of site: the thermodynamics of the system is represented by a single-site Langmuir isotherm at high temperatures and by a dual-site Langmuir isotherm at low temperature. At very low temperature a first order diffuse phase transition takes place around a loading interval in which the properties of the system change from a situation where the model behaves essentially as an ensemble of only inner sites, to a situation where

the model behaves essentially as an ensemble of only exit sites.

In conclusion, we have developed a general LGCA where the internal rules must satisfy the constraint of a *locality principle*.[34] The simplicity of our LGCA facilitates not only the simulations but also the theoretical analysis of structural and transport phenomena in such systems. We required that (a) at each time step the total number of accessible states of the lattice is the product of the number of accessible states of each cell that describes the *local* degrees of freedom, and (b) the Hamiltonian only involves *local* interactions. The advantage of our LGCA compared with other methods is that it provides a simplified description of the microscopic dynamics of particles adsorbed in micropore, yet most of the interesting details are intrinsically present and sometimes it is easier to see important correlations that are obscured in other methods. In this context our LGCA can be considered as the computationally cheapest model that has the essential properties of particles adsorbed in a micropore.

ACKNOWLEDGMENTS

This work has been carried out with financial support provided by Italian Ministero dell'Istruzione, dell'Università e della Ricerca, by Università degli Studi di Sassari, by INSTM, and by the COSMOLAB Consortium (CYBERSAR Supercomputing Research Project).

APPENDIX A: DETAILED BALANCE

If the randomization is microscopically reversible independently in each cell [i.e., it obeys detailed balance with respect to the energy function H defined in Eq. (3)], then it will be microscopically reversible also in the entire system. We make clear this statement through the following example.

For simplicity, we drop the time variable t, assumed fixed, and we label the cells by the subscripts $j=1,\ldots,M$ instead of the lattice vectors $\mathbf{r}$. Then we denote a system configuration having the cell 1 in the local configuration $\mathbf{s}_1$, the cell 2 in the local configuration $\mathbf{s}_2,\ldots$, the cell M in the local configuration $\mathbf{s}_M$, with

$$\bigcup_j \mathbf{s}_j \equiv \{\mathbf{s}_1,\mathbf{s}_2,\ldots,\mathbf{s}_M\}, \tag{A1}$$

where the index j runs from 1 to M. We made use of the notation $\cup_j \mathbf{s}_j = \mathbf{s}_1 \cup \mathbf{s}_2 \cdots \cup \mathbf{s}_M$ to indicate the union of the events $\mathbf{s}_1,\mathbf{s}_2,\ldots,\mathbf{s}_M$ constituting the configuration $\{\mathbf{s}_1,\mathbf{s}_2,\ldots,\mathbf{s}_M\}$.[35]

For each cell j, the randomization maps its input configuration $\mathbf{s}_j$ onto a new local configuration $\mathbf{s}_j^R$; therefore the configuration of the entire system will be mapped onto

$$\bigcup_j \mathbf{s}_j^R \equiv \{\mathbf{s}_1^R,\mathbf{s}_2^R,\ldots,\mathbf{s}_M^R\}.$$

Now we focus on a particular cell of the system, denoted k. We introduce the following probabilities:

- $p(\cup_j \mathbf{s}_j)$: probability of the system being in the configuration $\cup_j \mathbf{s}_j$;
- $p(\mathbf{s}_k | \cup_{j\neq k} \mathbf{s}_j)$: conditional probability of the single cell k being in the local configuration $\mathbf{s}_k$ when the rest of the system is in the configuration

$$\bigcup_{j\neq k} \mathbf{s}_j \equiv \{\mathbf{s}_1,\ldots,\mathbf{s}_{k-1},\mathbf{s}_{k+1},\ldots,\mathbf{s}_M\}.$$

For the cell k the detailed balance reads

$$p(\mathbf{s}_k|\cdot)R(\mathbf{s}_k \to \mathbf{s}_k^R) = p(\mathbf{s}_k^R|\cdot)R(\mathbf{s}_k^R \to \mathbf{s}_k), \tag{A2}$$

where we adopted the character "·" to indicate that the randomization rule is *blind* with respect to the input $(\cup_{j\neq k}\mathbf{s}_j)$ and output $(\cup_{j\neq k}\mathbf{s}_j^R)$ configurations of the rest of the system. If we take two particular cells k_1 and k_2, since they randomize independently of each other we can write

$$\begin{aligned} &p(\mathbf{s}_{k_1} \cup \mathbf{s}_{k_2}|\cdot)R(\mathbf{s}_{k_1} \to \mathbf{s}_{k_1}^R)R(\mathbf{s}_{k_2} \to \mathbf{s}_{k_2}^R) \\ &\quad = p(\mathbf{s}_{k_1}^R \cup \mathbf{s}_{k_2}^R|\cdot)R(\mathbf{s}_{k_1}^R \to \mathbf{s}_{k_1})R(\mathbf{s}_{k_2}^R \to \mathbf{s}_{k_2}). \end{aligned} \tag{A3}$$

Iterating we obtain

$$p\left(\bigcup_j \mathbf{s}_j\right)\prod_j R(\mathbf{s}_j \to \mathbf{s}_j^R) = p\left(\bigcup_j \mathbf{s}_j^R\right)\prod_j R(\mathbf{s}_j^R \to \mathbf{s}_j). \tag{A4}$$

Obviously if Eq. (A4) is satisfied then the energy balance

$$p(H_{\mathrm{sys}})R(H_{\mathrm{sys}} \to H_{\mathrm{sys}}^R) = p(H_{\mathrm{sys}}^R)R(H_{\mathrm{sys}}^R \to H_{\mathrm{sys}}), \tag{A5}$$

where H_{sys} and H_{sys}^R are, respectively, the pre- and the postrandomization energy of the system, is also satisfied.

Not only the randomization but also the entire randomization-propagation algorithm satisfies the detailed balance in the entire system.

- During randomization, the system performs a transition between an input configuration $\cup_j \mathbf{s}_j$ (with energy H_{sys}) and a postrandomization configuration $\cup_j \mathbf{s}_j^R$ (with energy H_{sys}^R) in a reversible way.
- Next the propagation step performs the allowed displacements *only* in the exit sites in a reversible way, because (i) the propagation probability p^P is symmetric [see Eq. (15)], and (ii) the total number of particles occupying the exit sites and the total number of particles occupying the inner sites are conserved separately during propagation, so the postpropagation energy of the system equals the postrandomization value: $H_{\mathrm{sys}}^R = H_{\mathrm{sys}}^P$.

So the following scheme applies:

$$H_{\mathrm{sys}}(t) \rightleftharpoons H_{\mathrm{sys}}^R(t) = H_{\mathrm{sys}}^P(t), \tag{A6}$$

where $\rightleftharpoons$ indicates that the randomization changes the energy of the system in a (probabilistically) reversible way, and $H_{\mathrm{sys}}^P(t) \equiv H_{\mathrm{sys}}(t+\tau)$, that is, the energy of the state of the system at time $t+\tau$, is defined as the energy of the postpropagation state at time t. Since the path (A6) from $H_{\mathrm{sys}}(t)$ to $H_{\mathrm{sys}}(t+\tau)$ satisfies the detailed balance, and there is no net drift in the motion of the particles [see Eq. (15)], then the model samples the equilibrium distribution of states in the long-time limit.

APPENDIX B: COMPUTATION OF THE PARTITION FUNCTIONS

Let us consider first the possible configurations of the N particles in the KM sites of the lattice $\mathcal{L}$. For a given configuration, let N_{ex} and N_{in} be the total number of occupied exit and inner sites, respectively. Obviously their sum is always the total number of particles $N=N_{ex}+N_{in}$, which is constant in time.

Since there is no interaction between the particles, the energy of the entire system depends only on the values of N_{ex} and N_{in}. As (n_{ex},n) defined in Sec. II B specifies a particular energy level of the single cell, in the same way we indicate as (N_{ex},N) a particular energy level of the system with degeneracy $\Omega(N_{ex},N)=\binom{M\nu}{N_{ex}}\binom{M(K-\nu)}{N-N_{ex}}$, where M is the total number of cells. The energy of the level (N_{ex},N) is

$$H_{sys}(N_{ex},N)=N_{ex}(\varepsilon_{in}-\varepsilon_{ex})-N\varepsilon_{in}. \tag{B1}$$

Therefore the Eq. (4) can be rewritten as

$$Q^{sys}=\sum_{N_{ex}=0}^{M\nu}\Omega(N_{ex},N)e^{-\beta H_{sys}(N_{ex},N)}. \tag{B2}$$

The probability of the level (N_{ex},N) is

$$\frac{\Omega(N_{ex},N)e^{-\beta H_{sys}(N_{ex},N)}}{Q^{sys}}, \tag{B3}$$

and the occupancy probability distribution of the single cell, indicated as

$$f^{eq}=\{f^{eq}(0),\ldots,f^{eq}(K)\},$$

reads

$$f^{eq}(n)=\frac{1}{Q^{sys}}\sum_{N_{ex}=0}^{M\nu}\sum_{n_{ex}=0}^{\nu}\binom{\nu}{n_{ex}}\binom{(M-1)\nu}{N_{ex}-n_{ex}}\binom{K-\nu}{n-n_{ex}}\times\binom{(M-1)(K-\nu)}{N-N_{ex}-n+n_{ex}}e^{-\beta H_{sys}(N_{ex},N)}. \tag{B4}$$

Computing probability distributions of states through Eqs. (B2) and (B4) is feasible only for a system containing a very small number of cells.

Instead, it is much easier to compute the probability distribution f^{eq} in terms of the cellular partition function, Z.

Let us denote[36] $\mathbf{a}=\{a_0,\ldots,a_K\}$ a particular distribution *of occupancies* of the system of M cells, where a_n is the number of cells having occupancy n.

- Given the particular distribution of occupancies $\mathbf{a}$, the sum over states of an ordered sequence of the M cells preserving the occupancy of each cell is $\Pi_{n=0}^{K}[Q^{cell}(n)]^{a_n}$.
- Differently ordered sequences of the M cells according to the distribution $\mathbf{a}$ are equally probable. The number of ways that any particular distribution of the a_j's can be realized is $M!/\Pi_{n=0}^{K}a_n!$.

Therefore the sum over states for a system described by the particular distribution of occupancies $\mathbf{a}$ is

$$W(\mathbf{a})=M!\prod_{n=0}^{K}\frac{[Q^{cell}(n)]^{a_n}}{a_n!}. \tag{B5}$$

Indicating as W^{TOT} the sum over states over all the possible configurations, for a very large system $(M\to\infty)$ we have

$$\lim_{M\to\infty}W^{TOT}=\lim_{M\to\infty}\sum_{\mathbf{a}}W(\mathbf{a})\approx W(\mathbf{a}^{eq}), \tag{B6}$$

where $\mathbf{a}^{eq}=Mf^{eq}$ is the equilibrium occupancy distribution. Using Stirling's approximation Eq. (B5) becomes

$$\ln W(\mathbf{a}^{eq})=M\ln M-\sum_{n=0}^{K}a_n^{eq}\ln a_n^{eq}+\sum_{n=0}^{K}a_n^{eq}\ln Q^{cell}(n). \tag{B7}$$

We maximize this function using the method of Lagrange multipliers with the constraints $\Sigma_{n=0}^{K}a_n^{eq}=M$ and $\Sigma_{n=0}^{K}na_n^{eq}=N$ and then we obtain Eq. (6).

The cellular partition function is written as $Z=\Sigma_{n=0}^{K}Q^{cell}(n)e^{\beta\mu n}$. This partition function is analogous to the grand-canonical one, so the following relations are satisfied:

$$\langle n\rangle=\frac{1}{\beta}\frac{\partial\ln Z}{\partial\mu}, \tag{B8}$$

$$\sigma^2(\langle n\rangle)=\frac{1}{\beta}\frac{\partial\langle n\rangle}{\partial\mu}, \tag{B9}$$

where $\sigma^2(\langle n\rangle)$ is the variance of the occupancy distribution f^{eq} at the loading $\langle n\rangle$.

Since the energy parameters ε_{ex} and ε_{in} are fixed in space and time, the expression for Z can be manipulated[36] to obtain the partition function of the Fermi-Dirac statistics:

$$Z=\prod_{j=1}^{K}(1+e^{\beta(\mu+\varepsilon_j)}), \tag{B10}$$

which reduces to Eq. (7). Now, using the relation (B8) and introducing the absolute activity $\lambda_a=e^{\beta\mu}$, we obtain the dual-site Langmuir isotherm reported in Eq. (8).

APPENDIX C: LIMITING OCCUPANCY DISTRIBUTIONS

1. Distributions for $T\to\infty$

In this case, $\lim_{T\to\infty}f^{eq}=f^{hyp}$, i.e., the particles distribute into the cells according to the hypergeometric distribution:

$$f^{hyp}(n)=\binom{K}{n}\binom{K(M-1)}{N-n}\Big/\binom{MK}{N}. \tag{C1}$$

For systems with a very large number of cells $(M\to\infty)$, this expression reduces to

$$f^{hyp}(n)=\binom{K}{n}(\rho)^n(1-\rho)^{K-n}, \tag{C2}$$

with $\rho=\langle n\rangle/K$. This is because in the limit of $T\to\infty$, Eq. (22) has the solution $\rho_{ex}=\rho_{in}=\rho$. The partition function of a closed cell reduces to $Q^{cell}(n)=\binom{K}{n}$, and Eq. (10) reduces to

$$f^{\mathrm{eq}}(n) = \binom{K}{n} \frac{\lambda_a^n}{(1+\lambda_a)^K}. \tag{C3}$$

Using the fact that $\rho = \lambda_a/(1+\lambda_a)$, we recognize in Eq. (C3) the hypergeometric distribution in the limit of $M \to \infty$ reported in Eq. (C2).

Using Eq. (B9) we obtain the variance

$$\sigma^2_{\mathrm{hyp}} = \frac{1}{\beta}\frac{\partial\langle n\rangle}{\partial\lambda_a}\frac{\partial\lambda_a}{\partial\mu} = -\frac{\langle n\rangle^2}{K} + \langle n\rangle. \tag{C4}$$

2. Distributions for $T \to 0$

In such a case the occupancy distribution splits up in two distinct hypergeometrics (referred to two distinct regions of loading) separated by a delta function at the loading at which the point transition (see Sec. V B) occurs:

$$\lim_{T\to 0} f^{\mathrm{eq}}(n) = \begin{cases} f^{\mathrm{hyp}}_{\mathrm{in}}(n) & \text{for } 0 \leqslant \langle n\rangle < K-\nu \\ \delta(n-\langle n\rangle) & \text{for } \langle n\rangle = K-\nu \\ f^{\mathrm{hyp}}_{\mathrm{ex}}(n) & \text{for } K-\nu < \langle n\rangle \leqslant K, \end{cases} \tag{C5}$$

where

$$f^{\mathrm{hyp}}_{\mathrm{in}}(n) = \binom{K-\nu}{n} (\rho_{\mathrm{in}})^n (1-\rho_{\mathrm{in}})^{K-\nu-n} \quad \text{with } \rho_{\mathrm{in}} = \frac{\langle n\rangle}{K-\nu}, \tag{C6}$$

and

$$f^{\mathrm{hyp}}_{\mathrm{ex}}(n) = \binom{\nu}{n-K+\nu} (\rho_{\mathrm{ex}})^{n-K+\nu} (1-\rho_{\mathrm{ex}})^{K-n} \quad \text{with } \rho_{\mathrm{ex}} = 1 - \frac{K-\langle n\rangle}{\nu}. \tag{C7}$$

This is because in the limit of $T \to 0$, Eq. (22) has the solutions (i) $\rho_{\mathrm{ex}}=0$ and (ii) $\rho_{\mathrm{in}}=1$. Using the relation

$$\langle n\rangle = \nu\rho_{\mathrm{ex}} + (K-\nu)\rho_{\mathrm{in}}, \tag{C8}$$

we find that, since $0 \leqslant \rho_{\mathrm{ex}} \leqslant 1$ (with $\alpha = \mathrm{ex}, \mathrm{in}$).

(i) If $\rho_{\mathrm{ex}}=0$, then $\langle n\rangle = (K-\nu)\rho_{\mathrm{in}}$, which is valid for $0 \leqslant \langle n\rangle < K-\nu$.
Since n_{ex} cannot be negative, then in order to satisfy the relation $\rho_{\mathrm{ex}}=0$ it must be $n_{\mathrm{ex}}=0$ for each occupancy $n = n_{\mathrm{ex}} + n_{\mathrm{in}}$. Therefore $n \in [0, K-\nu] \in \mathbb{N}$, and $Q^{\mathrm{cell}}(n)$ reduces to

$$Q^{\mathrm{cell}}_{\mathrm{in}}(n_{\mathrm{in}}) = \binom{K-\nu}{n_{\mathrm{in}}} e^{\beta\varepsilon_{\mathrm{in}} n_{\mathrm{in}}},$$

with $n_{\mathrm{in}} = n$. We can represent the sum over states in a cell through the inner partition function

$$Z_{\mathrm{in}} = (1 + e^{\beta\varepsilon_{\mathrm{in}}}\lambda_{\mathrm{in}})^{K-\nu}$$

[with $\lambda_{\mathrm{in}} = e^{\beta\mu_{\mathrm{in}}}$, with μ_{in} given by Eq. (20)]. Using Eq. (10) and the relation $n = n_{\mathrm{in}}$ we obtain

$$f^{\mathrm{eq}}_{\mathrm{in}}(n) = \binom{K-\nu}{n} \frac{(e^{\beta\varepsilon_{\mathrm{in}}}\lambda_{\mathrm{in}})^n}{(1+e^{\beta\varepsilon_{\mathrm{in}}}\lambda_{\mathrm{in}})^{K-\nu}}. \tag{C9}$$

Using the relation $\rho_{\mathrm{in}} = e^{\beta\varepsilon_{\mathrm{in}}}\lambda_{\mathrm{in}}/(1+e^{\beta\varepsilon_{\mathrm{in}}}\lambda_{\mathrm{in}})$, we obtain Eq. (C6). This is a hypergeometric distribution of particles in $K-\nu$ sites inside of a cell in the limit of $M \to \infty$, when the remaining ν sites are all empty. Its variance is

$$\sigma^2_{\mathrm{in}} = \frac{1}{\beta}\frac{\partial\langle n\rangle}{\partial\lambda_{\mathrm{in}}}\frac{\partial\lambda_{\mathrm{in}}}{\partial\mu_{\mathrm{in}}} = -\frac{\langle n\rangle^2}{K-\nu} + \langle n\rangle. \tag{C10}$$

(ii) If $\rho_{\mathrm{in}}=1$, since then $\langle n\rangle = \nu\rho_{\mathrm{ex}} + (K-\nu)$, which is valid for $K-\nu \leqslant \langle n\rangle < K$. Since n_{in} cannot be greater than $K-\nu$, then in order to satisfy the relation $\rho_{\mathrm{in}}=1$ it must be $n_{\mathrm{in}} = K-\nu$ for each occupancy n. Therefore $n \in [K-\nu, K] \in \mathbb{N}$. Since n_{in} is fixed, for each value of n also the observable n_{ex} turns out to be fixed. Therefore $Q^{\mathrm{cell}}(n)$ reduces to

$$Q^{\mathrm{cell}}_{\mathrm{ex}}(n_{\mathrm{ex}}) = e^{\beta\varepsilon_{\mathrm{in}}(K-\nu)} \binom{\nu}{n_{\mathrm{ex}}} e^{\beta\varepsilon_{\mathrm{ex}} n_{\mathrm{ex}}},$$

with $n_{\mathrm{ex}} = n - (K-\nu)$. Introducing $\lambda_{\mathrm{ex}} = e^{\beta\mu_{\mathrm{ex}}}$, we obtain the exit partition function

$$Z_{\mathrm{ex}} = e^{\beta\varepsilon_{\mathrm{in}}(K-\nu)}(1 + e^{\beta\varepsilon_{\mathrm{ex}}}\lambda_{\mathrm{ex}})^{\nu}.$$

Using Eq. (10) and the relation $n = K-\nu+n_{\mathrm{ex}}$, we obtain

$$f^{\mathrm{eq}}_{\mathrm{ex}}(n) = \binom{\nu}{n-K+\nu} \frac{(e^{\beta\varepsilon_{\mathrm{ex}}}\lambda_{\mathrm{ex}})^{n-K+\nu}}{(1+e^{\beta\varepsilon_{\mathrm{ex}}}\lambda_{\mathrm{ex}})^{\nu}}, \tag{C11}$$

which, using $\rho_{\mathrm{ex}} = e^{\beta\varepsilon_{\mathrm{ex}}}\lambda_{\mathrm{ex}}/(1+e^{\beta\varepsilon_{\mathrm{ex}}}\lambda_{\mathrm{ex}})$, can be reduced to Eq. (C7). This is a hypergeometric distribution of particles in ν sites inside of a cell in the limit of $M \to \infty$, when the other $K-\nu$ sites are all filled. Its variance is

$$\sigma^2_{\mathrm{ex}} = \frac{1}{\beta}\frac{\partial\langle n\rangle}{\partial\lambda_{\mathrm{ex}}}\frac{\partial\lambda_{\mathrm{ex}}}{\partial\mu_{\mathrm{ex}}} = -\frac{1}{\nu}[\langle n\rangle^2 - (2K-\nu)\langle n\rangle + K(K-\nu)]. \tag{C12}$$

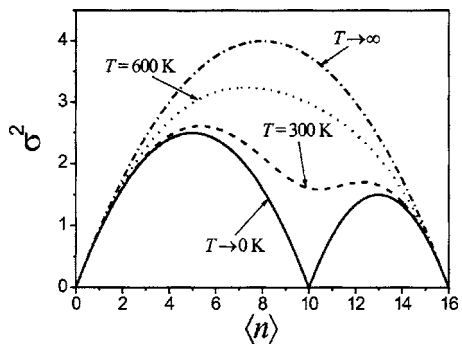

FIG. 11. The variance of the occupancy distributions at the two limiting temperatures $T \to \infty$ and $T \to 0$, and at the intermediate temperatures of 300 and 600 K.

(iii) At the transition point the relations $\rho_{ex}=0$ and $\rho_{in}=1$ hold simultaneously; therefore $f^{eq}=f_{in}^{hyp}\cap f_{ex}^{hyp}=\delta(n-\langle n\rangle)$ with $\langle n\rangle=K-\nu$.

In Fig. 11 the variance of f^{eq} at the two limiting temperatures [from Eqs. (C4), (C10), and (C12)] and at intermediate temperatures [obtained differentiating Eq. (8) with respect to μ at $T=300$ and 600 K] are shown. As can be seen, the properties of the distributions at $0<T<\infty$ are intermediate between the properties of the two limiting distributions, and temperature will determine to which of the two limiting distributions the f^{eq} will be more similar.

[1] *Recent Advances in Science and Technology of Zeolites and Related Materials*, Studies in Surface Science and Catalysis Vol. 154, Proceedings of the 14th International Zeolite Conference, Cape Town, South Africa, 25–30 April 2004, edited by E. Van Steen, L. H. Callanan, and M. Claeys (Elsevier, Amsterdam, 2004).

[2] J. Klafter and J. M. Drake, *Molecular Dynamics in Restricted Geometries* (Wiley, New York, 1989).

[3] A. Huwe, F. Kremer, P. Behrens, and W. Schwieger, Phys. Rev. Lett. **82**, 2338 (1999).

[4] *Fluid Transport in Nanoporous Materials*, NATO Science, Series II: Mathematics, Physics and Chemistry Vol. 219, Proceedings of the NATO Advanced Study Institute, La Colle sur Loup, France, 16–28 June 2003s, edited by W. Conner and J. Fraissard (Springer, Berlin, 2006).

[5] J. Kärger and D. M. Ruthven, *Diffusion in Zeolites and Other Microporous Materials* (Wiley, New York, 1992).

[6] P. Demontis, L. Fenu, and G. B. Suffritti, J. Phys. Chem. B **109**, 18081 (2005).

[7] P. Demontis, F. G. Pazzona, and G. B. Suffritti, J. Phys. Chem. B **110**, 13554 (2006).

[8] B. Chopard and M. Droz, *Cellular Automata Modeling of Physical Systems* (Cambridge University Press, Cambridge, England, 1998).

[9] J.-P. Boon, D. Dab, R. Kapral, and A. T. Lawniczak, Phys. Rep. **273**, 55 (1996); D. Dab, A. T. Lawniczak, J.-P. Boon, and R. Kapral, Simulation Practice and Theory **7**, 657 (2000).

[10] R. S. Drago, C. E. Webster, and J. M. McGilvray, J. Am. Chem. Soc. **120**, 538 (1998).

[11] W. Zhu, F. Kapteijn, and J. A. Moulijn, Phys. Chem. Chem. Phys. **2**, 1989 (2000).

[12] A. J. Skoulidas and D. S. Sholl, J. Phys. Chem. A **107**, 10132 (2003).

[13] R. Krishna, D. Paschek, and R. Baur, Microporous Mesoporous Mater. **76**, 233 (2004).

[14] D. Dubbeldam, E. Beerdsen, T. J. H. Vlugt, and B. Smit, J. Chem. Phys. **122**, 224712 (2005).

[15] Z. Chvoj, H. Conrad, V. Cháb, M. Ondrejcek, and A. M. Bradshaw, Surf. Sci. **329**, 121 (1995); Z. Chvoj, H. Conrad, and V. Cháb, *ibid.* **376**, 205 (1997).

[16] A. A. Tarasenko and L. Jastrabík, Surf. Sci. **507–510**, 108 (2002); N. A. Tarasenko, A. A. Tarasenko, Z. Bryknar, and L. Jastrabík, *ibid.* **562**, 22 (2004).

[17] A. N. Fitch, H. Jobic, and A. J. Renouprez, J. Phys. Chem. **90**, 1311 (1986).

[18] P. Demontis, S. Yashonath, and M. L. Klein, J. Chem. Phys. **93**, 5016 (1989).

[19] M. Kotrla, Comput. Phys. Commun. **97**, 82 (1996).

[20] S. Y. Bhide and S. Yashonath, J. Chem. Phys. **111**, 1658 (1999). S. Y. Bhide and S. Yashonath, J. Phys. Chem. B **104**, 2607 (2000).

[21] S. Fritzsche, R. Haberlandt, J. Kärger, H. Pfeifer, and M. Wolfsberg, Chem. Phys. Lett. **198**, 283 (1992).

[22] D. M. Ruthven, *Principles of Adsorption and Adsorption Processes* (Wiley, New York, 1984), Chaps. 2 and 3.

[23] G. B. Woods and J. S. Rowlinson, J. Chem. Soc., Faraday Trans. 2 **85**, 765 (1989).

[24] P. Demontis and G. B. Suffritti, Chem. Phys. Lett. **223**, 355 (1994).

[25] M.-O. Coppens, A. T. Bell, and A. K. Chakraborty, Chem. Eng. Sci. **53**, 2053 (1998).

[26] J. S. Rowlinson and G. B. Woods, Physica A **164**, 117 (1990).

[27] T. T. P. Cheung, J. Phys. Chem. **97**, 8993 (1993).

[28] C. J. Jameson, Annu. Rev. Phys. Chem. **47**, 135 (1996); M. Hunger and E. Brunner, in *Characterization I-NMR Spectroscopy*, Molecular Sieves: Science and Technology Vol. 4, edited by H. G. Karge and J. Weitkamp (Springer-Verlag, Heidelberg, 2004), pp. 201–293.

[29] J. Guemez and S. Velasco, Am. J. Phys. **55**, 154 (1987).

[30] R. Gomer, Rep. Prog. Phys. **53**, 917 (1990).

[31] C. J. Jameson, Mol. Phys. **102**, 723 (2004).

[32] E. Beerdsen, D. Dubbeldam, and B. Smit, J. Phys. Chem. B **110**, 22754 (2006).

[33] *Microscopic Simulations of Complex Hydrodynamic Phenomena*, NATO ASI Series, Series B: Physics Vol. 292, Proceedings of the NATO Advanced Study Institute, held in Alghero, Sardinia, Italy, 15–27 July 1991, edited by M. Marechal and B. L. Holian (Plenum, New York, 1992), Chap. III.

[34] G. Mack, Commun. Math. Phys. **219**, 141 (2001).

[35] R. Durrett, *The Essentials of Probability* (Duxbury, Belmont, 1994).

[36] D. A. MacQuarrie, *Statistical Mechanics* (Harper and Row, New York, 1976).